Classical and Quantum Transition State Theory for the Diffusion of Helium in Silica Sodalite

Michael J. Murphy,† Gregory A. Voth,‡ and Amy L. R. Bug*,†

Department of Physics and Astronomy, Swarthmore College, Swarthmore, Pennsylvania 19081, and Department of Chemistry, University of Pennsylvania, Philadelphia, Pennsylvania 19104-6323

Received: July 11, 1996; In Final Form: October 14, 1996[⊗]

We use a classical transition state theory (TST) to calculate the diffusion constant for noble gas atoms through silica sodalite. Due to the restrictive geometry of the transition state, diffusion of Ne and Ar is energy-activated at room temperature, but the diffusion of He is limited by entropy. The small mass of He suggests that a quantum TST must be employed. Path integral Monte Carlo is used to perform the relevant sampling, and quantum and classical diffusivities are compared. Comparison reveals a competition between tunneling and diffraction of the quantum mechanical He atom. A pairwise centroid pseudopotential is developed for the guest−host atom pair, and the effective potential energy and TST rate are compared with that of direct quantum TST.

1. Introduction

Zeolites are microporous solids with a variety of laboratory and industrial applications.[1] With their regular systems of microscopic cages and channels, they are useful as filters, as drying media, as solid catalysts for chemical reactions, and safe, capacious storage media for gases like methane and hydrogen. The mobility of a guest molecule within a zeolite is relevant to all of these applications, and a number of recent books and review articles treat the important topic of guest diffusion in zeolites.[2] In this paper, we use computer simulation to study the intracrystalline diffusion of the noble gas atoms He, Ne, and Ar in sodalite, a zeolite with small cages suited to the encapsulation[3] and storage[4] of small guests. Noble gas atoms are frequently treated as zeolitic guests in modeling studies. Not only does their simplicity facilitate analysis, but the real-world processes of purification of gas streams, the removal of radioactive off-gases as a byproduct of nuclear fission,[5] and NMR characterization of solids using ^{129}Xe [6] all involve these guests in zeolites.

For a highly heterogenous host like a zeolite, the challenge is to identify the dominant features that control the nature of the diffusive process.[2,7] For some host−guest systems, simplified models of smooth pores may be appropriate, and bulk diffusion (typically, at high density) or Knudsen diffusion (low density) within them is an appropriate model.[8,9] (Complicating this picture slightly, there may be a crossover between bulk and Knudsen dynamics at some locations in the host structure; the experimental result is an interpolation between the two behaviors.[10]) Other simplified potential models (e.g. a 3D sinusoidal[11] variation) produce exact results for D and can reproduce experiment very well in certain hosts.[9] Finally, for tightly confined guests, the effects of the walls may be felt throughout the region through which the guest travels, and molecular walls must be adequately modeled. Diffusion is often activated in such cases. A typical situation of activated diffusion is one that enables passage through an aperture of the same size as the kinetic diameter of the guest.[9] Another case one might encounter: strong attractive interactions between atoms (particularly ions) on the zeolite's internal "surface" and guests may imply activated diffusion.[12] In this case, the attractive wells between which activated diffusers "jump" need not be centered on single atoms; rather, wells may exist in rings or from the superposed interaction of regions of zeolite channels, as the numerous simulations of guests in silicalite have shown.[13−15] The solid in the present study, silica sodalite (see section 4), is nonpolar, with a framework structure that is very similar to the naturally-occuring polar form: the aluminosilicate, sodium sodalite. It has no channels, but apertures lead directly between "sodalite" cages. Guests are tightly confined, and we will examine the model of diffusional control by activated diffusion through apertures.

In this paper, we consider the diffusion of single guests (hence the dilute, Henry's law limit) in the host. We use transition state theory (TST), outlined in sections 2 and 3, to predict guest diffusion constants. This approximate theory will, in our case, estimate the rate at which the guest traverses apertures between cages. When computationally feasible (i.e., for He at room temperature) we compare TST with the results of full dynamical simulation, and for this case the dynamical corrections to TST (which render the theory exact) are discussed. The limitations of a classical treatment of He are pointed out in section 6, where a path integral representation of He is employed in a quantum TST. Finally, a pseudopotential is developed for the centroid of the He path in section 7. This might be used in either a statistical (TST) or dynamical treatment of the diffusion of He within the host solid.

2. Transition State Theory of Diffusion

The history of transition state theory (TST)[16,17] extends beyond its use in the context of chemical kinetics, though this is the field with which this theory is most closely identified. The thermally-activated escape of any classical system from a metastable state A can be estimated by the TST, or absolute rate, expression (first written in this form by Eyring[18,19]):

$$k_{\mathrm{TST}} = \frac{k_{\mathrm{B}}T}{h}\frac{Q^{\ddagger}}{Q_{\mathrm{A}}}\mathrm{e}^{-E^{*}/k_{\mathrm{B}}T} \tag{1}$$

This equation models escape from A over a potential barrier,

* Author to whom correspondence should be addressed.
† Swarthmore College.
‡ University of Pennsylvania. Current address: Department of Chemistry, University of Utah, Salt Lake City, UT 84112.
⊗ Abstract published in *Advance ACS Abstracts,* December 15, 1996.

S1089-5647(96)02067-6 CCC: $14.00

whose top represents the "transition state" (TS). E^* is the height of the barrier above the well A, Q_A and $Q^‡$ are partition functions in the well and TS, respectively (the latter being a reduced partition function which sums over all coordinates orthogonal to the direction leading from reactant A to product B), and the temperature T provides the driving force for escape. The TST approximation states that the rate is the current of reactant passing away from A through the TS, per unit of reactant in the well. It is predicated on the hypothesis that reactant is in thermal equilibrium at the reactant region. Conventional wisdom states that if $E^* \geq 5k_BT$, reactant will not be depleted too quickly and equilibrium will hold.[20] Generalizations and extensions of the simple model of eq 1 are well-known. Among them are the following: (i) to other ensembles, particularly the microcanonical ensemble as in the work of Pechukas and Pollak;[21,22] (ii) to multiple dimensions—the TS is a hypersurface and the integration over nonreactive degrees of freedom results in E^* being related to a potential of mean force, rather than a bare potential energy;[23,24] (iii) to multiple TS surfaces leading to multiple product wells—diffusion on surfaces is a principal case, which will be discussed below. Also, note that in more than one dimension, the TS is often centered on a first-order saddle point of the potential surface, but this is not a requirement. The choosing of the location of the TS to produce the smallest (best estimate) k_{TST} has been the focus of detailed study.[22]

Equation 1 is only an approximation, which ignores the detailed dynamics of the reacting system. In particular, when nonreactive degrees of freedom include the motions of solvent molecules, the average effect of this "bath" can be imposed through an effective friction on the reaction coordinate. There exists an extensive literature, beginning with the work of Kramers,[25] on systematic corrections to TST in baths described by various friction kernels.[16,26] When one attempts to visualize what feature of the dynamics is missed by TST, it is the feature of nonreactive recrossings of the TS. So, one can write a phenomenological correction to TST, in which a great deal of dynamical information is condensed into a transmission coefficient κ:[27]

$$k = \kappa k_{TST} \tag{2}$$

Because it corrects for reactant trajectories which cross the TS from A, but ultimately fail to equilibrate in a product well, $\kappa \leq 1$.

One approach to the calculation of κ, and hence the exact rate k, is the "reactive flux" formalism.[16,23] In terms of the reaction from state A into B, with q^* denoting the location of the TS, one defines a time-dependent rate in terms of this time correlation function of the reaction coordinate, $q(t)$:

$$k(t) = \langle \dot{q}(0)\, \delta(q(0))\, \theta_B(q(t)) \rangle \tag{3}$$

where $\langle ... \rangle$ is the usual thermal average. $k(t{=}0^+)$ is thus

$$k(0^+) = \langle \dot{q}(0)\, \delta(q(0))\, \theta_B(\dot{q}(0)) \rangle \equiv \langle |\dot{q}(0)| \delta(q(0)) \rangle /2 \tag{4}$$

and it can be shown that $k(0^+) \equiv k_{TST}$.[23,28] If there is a separation of time scales, so that correlated recrossings of the TS are completed in a time much less than the time to react, k^{-1}, eq 3 will plateau, and the plateau value is identified with the rate k.[23] This method is well suited to molecular dynamics simulation and has been applied with great success to simulations of liquid-state-type reactions.[29]

How does one adapt this theory to activated diffusion of guests in zeolites? TST has a natural role in the calculation of defect and tracer/guest diffusion rates in solids[30,31] and has long been used for this purpose.[32−34] Expressions like[35]

$$D = \frac{k_B T \delta^2}{6h} \frac{n Q^*_z}{Q_z} e^{(u_z - u^*_z)/k_B T} \equiv \frac{\delta^2}{6} n k_{TST} \tag{5}$$

for the self-diffusion constant of small molecules, at low densities, in zeolite A are based on a view of activated "hopping" from one state to another.[36] There are n equivalent states at a distance δ from the original state. The Q_z, Q^*_z are products of translational, vibrational, and rotational partition functions in the original state and in the TS leading to one target state, respectively; so the guest can hop to any *one* of these states with a rate which is k_{TST} of eq 1. While a few early studies on small molecules in zeolite A[37] failed to predict diffusion rates of the same order of magnitude as experiment, others[35] have done this quite successfully for a range of small molecules in the Henry's law regime. Results similar to those of Kramers theory were developed for diffusion of impurities on tungsten by Banavar et al.[38] (the friction arises from motion of the substrate atoms). The role of dynamical corrections to TST takes on an added dimension in the guest-diffusion problem. Not only are there the usual correlated recrossings of a single TS, but there are correlated hops from one well to another; the guest might not equilibrate until several intermediate states are traversed.[39] So while one can define a dynamically corrected k of exactly the form of eq 2, it is not required that this multistate transmission coefficient, κ, is less than unity. Both TST predictions and the corrective results of dynamical simulations were examined by Bennett[31] for defect diffusion in LJ solids. In a series of papers, Voter and Doll used uncorrected TST[40] and then derived and used a formalism for multistate dynamically corrected TST[41] for adatoms on solid surfaces. Their formalism succeeds in describing surface diffusion[41,42] and has also been used in guest/zeolite systems where dynamical corrections were shown to be nonnegligible.[14,43]

3. Quantum Transition State Theory

For the light guest He, we will find (section 6) that its mobility should be investigated quantum mechanically. There are several alternative formulations of quantum TST (QTST).[16,44] In this paper, we will rely on the path integral quantum TST (PI-QTST) formalism.[45] This approach is rooted in Feynman's path integral formulation of quantum statistical mechanics.[46] To review the main points briefly: the fundamental operator of equilibrium statistical mechanics, the density matrix $\hat{\rho}(\beta) = e^{-\beta \hat{H}}$, where $\beta = 1/k_BT$ and $\hat{H}$ is the Hamiltonian, is related to the canonical partition function via $Q = \mathrm{Tr}\hat{\rho}(\beta)$. Writing this in the coordinate representation:

$$Q = \int \langle \mathbf{x} | \hat{\rho}(\beta) | \mathbf{x} \rangle \, d\mathbf{x} \tag{6}$$

where $\mathbf{x}$ is a coordinate describing N degrees of freedom of the system. One can argue[47] as follows: Its definition implies that $\hat{\rho}(\beta) = \prod^P \hat{\rho}(\epsilon)$ where $\epsilon = \beta/P$. One can then insert a complete set of coordinate states between each of the terms in this product, to arrive at

$$Q = \int \langle \mathbf{x} | \hat{\rho}(\epsilon) | \mathbf{x}_1 \rangle \langle \mathbf{x}_1 | \hat{\rho}(\epsilon) | \mathbf{x}_2 \rangle ... \langle \mathbf{x}_{P-1} | \hat{\rho}(\epsilon) | \mathbf{x} \rangle \, d\mathbf{x} \, d\mathbf{x}_1 \, ... \, d\mathbf{x}_{P-1} \tag{7}$$

In the limit that $P \rightarrow \infty$, each thermal density matrix element in the integrand of eq 7 becomes

$$\langle \mathbf{x} | \hat{\rho}(\epsilon) | \mathbf{x}' \rangle \approx \langle \mathbf{x} | \hat{\rho}_{free}(\epsilon) | \mathbf{x}' \rangle e^{-\epsilon U(x)} \tag{8}$$

where U is the potential energy function and the free propagator $\hat{\rho}_{\text{free}}$ is a Gaussian:

$$\langle \mathbf{x}|\hat{\rho}_{\text{free}}(\epsilon)|\mathbf{x}'\rangle \propto \exp\left[-\frac{m}{2\hbar^2\epsilon}(\mathbf{x}-\mathbf{x}')^2\right] \tag{9}$$

This is a high temperature (classical) limit. The width of the Gaussian is approximately the deBroglie wavelength at temperature k_B/ϵ of a particle of mass m (the generalization to distinct masses for each degree of freedom is straightforward.) The center lies at $\mathbf{x} = \mathbf{x}'$.

Formally, one could write

$$Q = \int \mathrm{e}^{-S[\mathbf{x}(\tau)]/\hbar}\, D\mathbf{x}(\tau) \tag{10}$$

where τ is an imaginary time and S is the action functional:[46]

$$S[\mathbf{x}(\tau)] = \int_0^{\hbar\beta}\left[\frac{m}{2}\dot{\mathbf{x}}^2 + U(\mathbf{x})\right]\mathrm{d}\tau \tag{11}$$

But for computational purposes, eqs 7−9 are extremely useful as written. (They use the so-called "primative propagator"; the simplest approximation which converges to the true propagator in the large P limit.) They reflect the isomorphism of the quantum partition function to the classical partition function of a ring polymer, first pointed out by Chandler and Wolynes.[48] Sampling techniques, either Monte Carlo (MC) or MD, that allow one to determine the free energy of a cyclic polymer with P "beads" (monomers) joined by harmonic bonds will allow one to compute Q for the isomorphic quantum particle. Explicitly, in the large P limit,

$$Q = \left(\frac{mP}{2\pi\beta\hbar^2}\right)^{NP/2}\int \delta(\mathbf{x}_0 - \mathbf{x}_P)\exp\left[-\frac{mP}{2\beta\hbar^2}\sum_{i=1}^{P}(x_i - x_{i-1})^2 - \frac{\beta}{P}\sum_{i=1}^{P}U(\mathbf{x}_i)\right]\mathrm{d}\mathbf{x}_0\,\mathrm{d}\mathbf{x}_1 \ldots \mathrm{d}\mathbf{x}_P \tag{12}$$

Note that if the N degrees of freedom involve M classically indistinguishable particles, one multiplies eq 12 by an additional factor of $1/M!$ (Gibbs paradox). U accounts for not only interactions with an external field but also classical interactions between beads on different ring polymers.

The centroid of a path $\mathbf{x}(\tau)$ which contributes to the integral above is

$$\tilde{\mathbf{x}}_0 = \frac{1}{P}\sum_{i=1}^{P}\mathbf{x}_i \tag{13}$$

For problems in quantum activated transport, the importance of variations in the free energy with centroid location was appreciated[49] before its role in QTST was rigorously defined as follows.[45] One defines a centroid-constrained free energy, F_c, and a corresponding density, Z_c, as

$$\mathrm{e}^{-F_c(\mathbf{x}_c)/k_BT} \equiv Z_c(\mathbf{x}_c) = \int \delta(\tilde{\mathbf{x}}_0 - \mathbf{x}_c)\langle \mathbf{x}|\hat{\rho}(\epsilon)|\mathbf{x}_1\rangle\langle \mathbf{x}_1|\hat{\rho}(\epsilon)|\mathbf{x}_2\rangle \ldots \langle \mathbf{x}_{P-1}|\hat{\rho}(\epsilon)|\mathbf{x}\rangle\,\mathrm{d}\mathbf{x}\,\mathrm{d}\mathbf{x}_1 \ldots \mathrm{d}\mathbf{x}_{P-1} = \int \delta(\tilde{\mathbf{x}}_0 - \mathbf{x}_c)\mathrm{e}^{-S[\mathbf{x}(\tau)]/\hbar}\, D\mathbf{x}(\tau) \tag{14}$$

Then the PI-QTST rate constant is simply

$$k_{\text{QTST}} = \frac{1}{2}\langle|v^*|\rangle\frac{Q^*_c}{Q_A} \tag{15}$$

where

$$Q^*_c = \int_{\text{TS}} Z_c(\mathbf{x}_c)\,\mathrm{d}S$$

is the partition function with the centroid constrained to lie on the (planar) TS hypersurface in configuration space. A justification appears in ref 45, though one can immediately see that eq 15 is a plausible quantum analog of k_{TST} in section 2. As before, $\langle|v^*|\rangle$ is assumed to take on its (classical) equipartitioned value, and Q_A is an unconstrained partition function for the reactant state.

4. Model

The locations of framework atoms (Si, O) of silica sodalite are taken from X-ray and neutron diffraction studies.[50] The dehydrated solid has a unit cell composition of $Si_{12}O_{24}$ and has cubic ($Im3m$) symmetry, with a lattice constant $a = 8.83$ Å. Our simulation employs 8 unit cells which form a 9-cage fragment of the lattice (Figure 1). As is common in the guest−zeolite literature, interactions are modeled as atom−atom, and interactions arising between the "T" atoms (Si in our case) and guests are neglected, thanks to the small van der Waals radii of the former. In the nonpolar, siliceous species, a simple Lennard-Jones interaction is often used:

$$U(\mathbf{r}) = \sum_i \frac{B}{|\mathbf{r} - \mathbf{r}_i|^{12}} - \frac{A}{|\mathbf{r} - \mathbf{r}_i|^6} \tag{16}$$

The sum is over all oxygen atom locations $\mathbf{r}_i$; the guest (He, Ne, or Ar) is at $\mathbf{r}$. The London dispersion constant A is chosen according to the semiempirical Slater−Kirkwood formula,[51] and B is chosen in the usual way, so that the potential minimum for a guest−host pair coincides with the correct van der Waals radius. Parameters of eq 16 are given in Table 1. They are in good agreement with those of ref 15, which also treats diffusion of noble gas guests in a rigid, siliceous zeolite (silicalite).

One might imagine that exchange of energy with a moving lattice is required in order to model the process of relaxation into a cage, and excitation to the TS. But as Haug et al.[52] saw in their surface-hopping study of hydrogen, relaxation, activated crossing, and recrossing all occurred due to the roughness of the atom−atom potential and the exchange of energy that could occur between parallel and perpendicular (nonreactive) modes of motion. Similarly, in a simulation of the diffusion of Xe on a Pt surface, Sholl and Skodje[53] were able to correlate the termination of a correlated section of trajectory with a peak in the energy of motion and position perpendicular to the surface. Relaxation into cages and diffusive motions were also well-defined processes in the rigid-disk gas model of Machta and Zwanzig.[54] So while a simulation with a moving lattice may be very worthwhile, one might expect a reasonably similar rate constant to arise in a simulation with a rigid lattice, especially if the lattice reflects the correct geometry of the TS (which may be perturbed by the guest).[42]

Figure 2 contains a potential map for He (Ne and Ar are qualitatively similar) within the sodalite cage. As is often done in potential computations, the LJ potential of eq 16 is truncated at a distance of 2.5σ ($\sigma = (B/A)^{1/6}$) for each pair of particles and is also shifted upwards so that the potential at this distance, and beyond, is zero. The plane, $y = z$, of the map is significant—it (along with $z = x$ and $x = y$) is the plane in which is located the "reaction coordinate" leading from a local minimum within a cage (M1 of Figure 2) through a saddle point (SP) to an M1 in the adjacent cage. By symmetry, there are eight equivalent M1 in each cage, which are interconnected through a steepest-descent path through six local minima (M2)

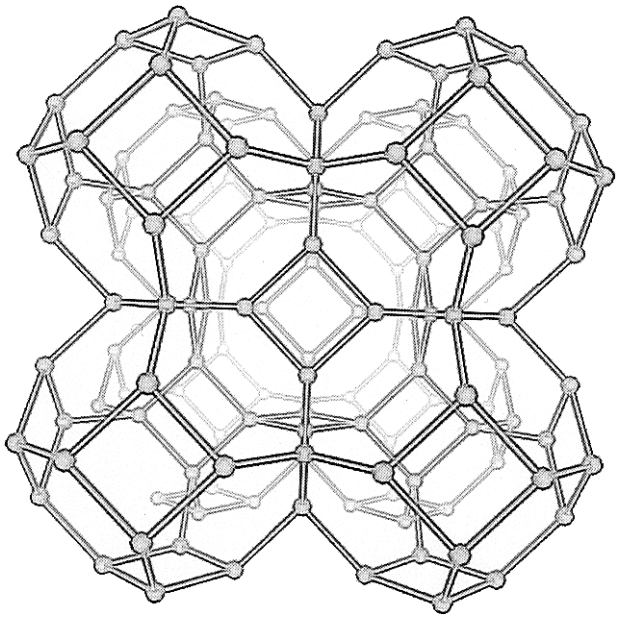

Figure 1. Fragment of silica sodalite lattice used in simulation. Small spheres are silicon atoms; bonds are drawn to show the connectivity between silicons that define the 14-sided "sodalite" cages, packed in a bcc arrangement. Oxygen atoms are not shown.

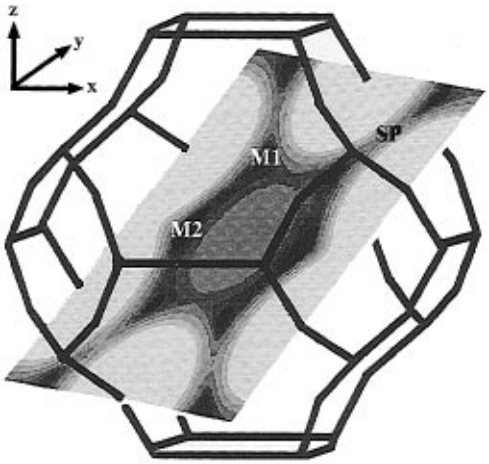

Figure 2. Potential map in $y = z$ plane for He in silica sodalite. Minima M2,M1 and saddle point SP on transition state surface are at −0.80, −0.75, and −0.30 kcal/mol, respectively.

TABLE 1: Parameters for Lennard-Jones Interaction between O and Guest

guest	vdW radius (Å)	A (kcal/mol Å^6)	B (kcal/mol Å^{12})
He	1.3	102	25 600
Ne	1.6	234	108 000
Ar	1.9	801	619 000

which are only slightly lower in energy. At the temperatures which we have studied ($T \geq 50$ K), localization in one of these minima is not considered as a distinct "state" of the guest. Rather, as has been discussed by several authors,[43,55] a state i is identified with residency in a particular cage, because crossing the low-lying saddle point between M1 and M2 is not rate limiting to the transport of the guest. Such low-lying saddles also exist in the study of June et al.[14] In the application of TST to diffusion, the reaction coordinate is a curve in coordinate space that leads the guest from one state into an adjacent one. Though there is no unique definition in the literature, we adopt a common one: the reaction coordinate is a steepest-descent path leading between minima in adjacent states, and passing through the saddle point. The potential field in sodalite is

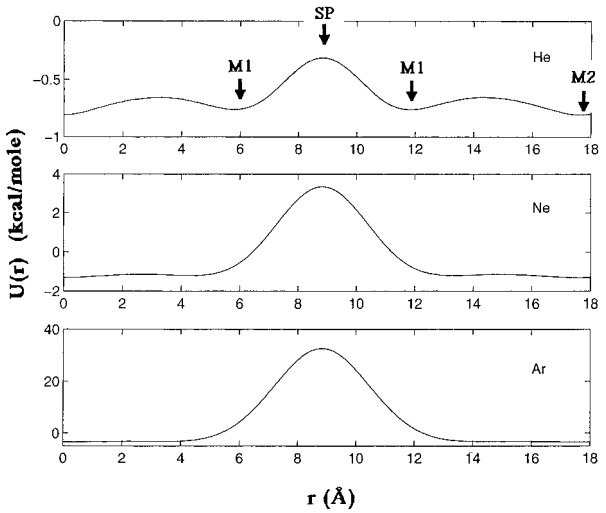

Figure 3. Potential energy along reaction coordinate, r, for He, Ne, and Ar. Locations of minima and SP corresponding to Figure 2 are marked.

sufficiently symmetrical, and the number of degrees of freedom of the system sufficiently small (3) that visualization software allows us to identify a plane (Figure 2) in which the reaction coordinate lies. The distance along the reaction coordinate is found to vary monotonically with the distance along the Cartesian axis (y or z in Figure 2) and this makes the search for the steepest-descent path straightforward. The transition state (TS) between states i and j, a surface normal to the reaction coordinate at the saddle point, is simply the planar region in the center of the O 6-ring that separates cages i and j.

5. Classical Rate of Diffusion

The potential along the reaction coordinate is given in Figure 3. The energy barrier across the saddle point is sufficiently high for Ne and Ar ($E^* \approx 2500$ K and 16 000 K, respectively) that cage-to-cage transport is expected to be energy activated at room temperature. For He, with $E^* \approx 250$ K, this is not the case. One may rewrite the simple TST expression eq 1 as

$$k_{\mathrm{TST}} = \frac{k_{\mathrm{B}}T}{h} \mathrm{e}^{-\Delta F^*/k_{\mathrm{B}}T} \tag{17}$$

to emphasize the fact that it is the free energy difference, $\Delta F^* = E^* - T\Delta S^*$, between the caged state and the transition state which determines the rate. To make an estimate of the importance of entropy vs energy activation, one may substitute for k_{TST} in eq 17 from eq 1 and performing integrations over momenta, one obtains the free energy difference

$$\mathrm{e}^{-\Delta F^*/k_{\mathrm{B}}T} = \frac{h}{(2\pi m k_{\mathrm{B}}T)^{1/2}} \frac{\int_{\mathrm{TS}} \mathrm{e}^{-U/k_{\mathrm{B}}T}\,\mathrm{d}S}{\int_{\mathrm{A}} \mathrm{e}^{-U/k_{\mathrm{B}}T}\,\mathrm{d}V} \tag{18}$$

in terms of integrals of the Boltzmann factor over the volume of the reactant cage (state A) and the TS surface respectively. Our TS surface is the eight planar faces of the cage doorways, and we should note that eq 18 would need to be generalized slightly[40] were this a case of a nonpiecewise-planar TS surface. Equation 18 was evaluated for temperatures in the range $T =$ 10−600 K. Thanks to the simplicity of the geometrical construction of the cage and TS, integrals were performed by simple quadrature, using 200 × 200 and 120 × 120 × 120 grids of points for the TS doorway and cage interior, respectively. From the temperature behavior of the calculated free energy

ΔF^*, values of $E^* = 190$ K and $\Delta S^* = 4$ eu were obtained. (It is not surprising that this activation energy is somewhat lower than the difference of 250 K between TS and M2, since it involves a thermal average over the cage.) This suggests that when $T\Delta S^* \geq E^*$, roughly $T \geq 50$ K, the reaction rate is limited by an entropy, rather than an energy, difference.

There are two other ways one might frame this argument. One is to examine the free energy integrated over small surfaces normal to the reaction coordinate, both in one of the wells, M, and in the TS. An early paper by Wert[33] on TST applied to impurity diffusion in solids reasons along these lines. Wert points that the following reframing of Eyring's expression is appropriate for this sort of system:

$$k_{\mathrm{TST}} = \nu \mathrm{e}^{-\Delta F^*_S/k_B T} \tag{19}$$

where

$$\mathrm{e}^{-\Delta F^*_S/k_B T} = \frac{\int_{\mathrm{TS}} \mathrm{e}^{-U/k_B T}\, \mathrm{d}S}{\int_{\mathrm{M}} \mathrm{e}^{-U/k_B T}\, \mathrm{d}S} \tag{20}$$

because it compares the free energy difference for a particle with the same number of degrees of freedom in the well and at the TS. (Thus, one may envision a simple process for which ΔF^*_S represents the reversible work.[34] Above, ν is a temperature-dependent factor, an effective frequency of oscillation in the well M and is derived from eq 1 by a partial integration of Q_A over the degree of freedom along the reaction coordinate.) A more technical approach which computes entropy in a similar way arises in the treatment of a pure entropy barrier by Zwanzig et al.[54,56] There, an approximate theory of diffusion in a channel of varying cross section is presented, the so-called "Fick−Jacobs" theory. The width of the channel at distance x along its axis is identified with $\mathrm{e}^{S(x)/k_B}$. This theory underlies our eq 20; x is the reaction coordinate and $S(x)$ is evaluated at the well and TS. A calculation was done for dS ranging over a small disk of radius 0.5, 1.0, or 2.0 Å and, for each radius, at temperatures in the range $T = 10-50$ K (eq 20 is not relevant for temperatures at which the guest spends much time far from M). Results for various radii were not significantly different, and with $\Delta F^*_S \equiv E^* - T(S(x{=}\mathrm{M2}) - S(x{=}\mathrm{TS}))$ a fit to eq 20 gives $E^* = 240$ K and $S(\mathrm{M2}) - S(\mathrm{TS}) = 3$ eu. Alternatively, also at low temperatures, one could estimate ΔS^* by calculating the partition functions in eq 1 in the harmonic approximation. This is done later in section 6. The conclusion from all of these back-of-the-envelope calculations is that for $T \approx 50$ K and above, the classical diffusion of He is entropy-limited, while the transport of Ne and Ar remains thermally activated at well above room temperature. Figure 4 is an isopotential plot which illustrates the entropic "bottlenecks" encountered by He at the cage doorways.

To find the rate of diffusion, eq 1 (alternatively, eqs 17 and 18) or eq 4 leads us to evaluate

$$k_{\mathrm{TST}} = \frac{1}{2}\langle|v^*|\rangle \frac{\int_{\mathrm{TS}} \mathrm{e}^{-U/k_B T}\, \mathrm{d}S}{\int_{\mathrm{A}} \mathrm{e}^{-U/k_B T}\, \mathrm{d}V} \tag{21}$$

for the guest within the zeolite. In eq 21, v^* is the component of the velocity perpendicular to the TS surface, and taking the canonical average brings one back to e.g. eq 17. If nonreactive recrossings and correlated hops beyond one cage are negligible (assumptions which will be examined later) k_{TST} will completely describe the diffusion constant:

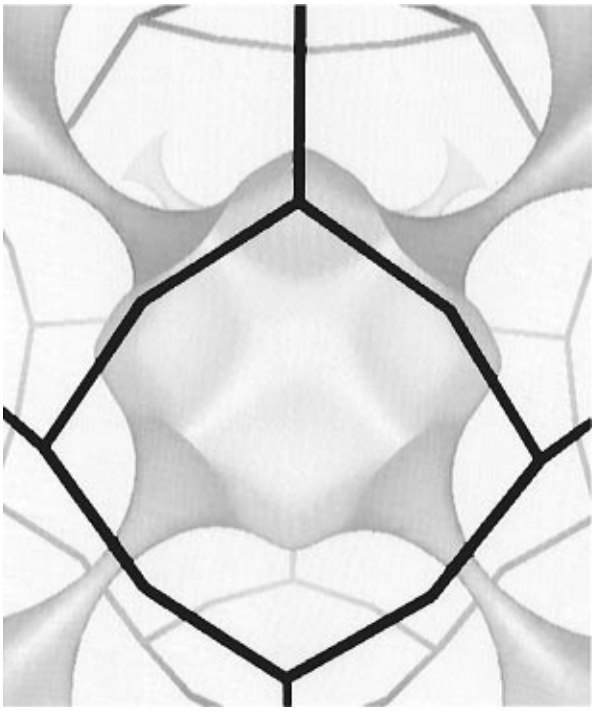

Figure 4. Isopotential plot for He in silica sodalite, for potential surface at −0.1 kcal/mol.

$$D_{\mathrm{TST}} = (\delta^2/6)k_{\mathrm{TST}} \tag{22}$$

where $\delta = a\sqrt{3}/2 = 7.65$ Å.

The integrals in eq 21 were evaluated, as mentioned above, via quadrature. In a more complicated geometry, the ratio of these integrals might be evaluated with Monte Carlo (MC). One allows the guest to perform a random walk in the host, biased by the Boltzmann factor $\mathrm{e}^{-U/k_B T}$, records the fraction of steps, f_w, that terminate within a disk of width w centered on the TS, and evaluates

$$k_{\mathrm{TST}} = \frac{1}{2}\langle|v^*|\rangle \lim_{w\to 0} \frac{f_w}{w} \tag{23}$$

This was the general approach taken in refs 14, 40, and 42; in some of these studies the biasing of the walk was supplemented by an importance sampling function to ensure adequate sampling of the intrinsically rare visits to the TS. Voter[57] has investigated such issues in detail. We have been able to double-check our quadrature calculations by evaluating eq 23, allowing He and Ne to perform random walks in a lattice with periodic boundary conditions and extrapolating linearly to $w = 0$ samples in the range $w = 0.4-0.02$ Å. Such MC sampling was of primary importance in quantum TST calculations described in section 6.

Diffusion constants at 300 K from classical TST are given in Table 2. Activation energies from an Arrhennius fit of eq 21 are also given for Ne and Ar; and they are in good agreement with what one would infer from the energy barrier heights in Figure 3. We know of no experimental data on diffusion of noble gas guests in silica sodalite, though data exist for Ar in the naturally-occurring sodium sodalite. Barrer and Vaughan[58] report activation energies of $E^* = 27$ and 30 kcal/mol from two different samples. Because Na^+ ions block on average three out of four cage doorways, we expect these to have a dramatic effect on diffusivity, and comparison of D is not useful between sodium and silica sodalite. Even for unblocked doorways, the locations of O atoms differ slightly between the two sodalites,

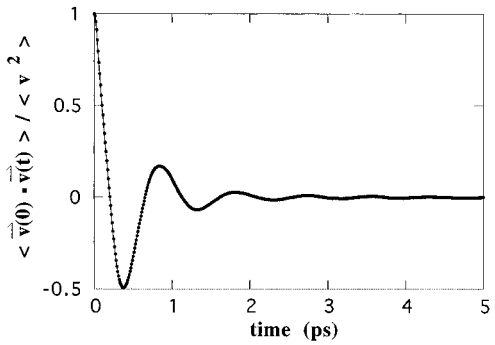

Figure 5. Normalized velocity autocorrelation function for He at 300 K. With relaxation modeled as exponential, the relaxation time, τ_{corr} is approximately 2 ps.

TABLE 2: Activation Energies, Room Temperature (300 K) Classical Diffusion Constants, and Cage Residency Times for Noble Gases in Silica Sodalite

guest	E^a (kcal/mol)	D_{TST} (Å^2/ps)	τ_{TST}	D_{MD} (Å^2/ps)
He		0.43	23 ps	0.38
Ne	5.0	7.1×10^{-5}	140 ns	
Ar	37	2.4×10^{-28}	*a*	

[a] Trapped on laboratory time scale.

varying with alumina content;[59] for this reason, and because our rigid structure does not permit relaxation of solid atoms at the TS, such rough agreement between experiment and the calculation is all one might expect.

From the cage residency times, $\tau_{TST} \equiv k_{TST}^{-1}$, one sees that it is prohibitively expensive, in terms of computer time, to explicitly simulate the diffusional motion of Ne (and larger noble gas guests) at room temperature. (Hence the utility of the TST approach.) He is sufficiently mobile that one may follow its motion with molecular dynamics (MD), and we have done so in order to compare the measured diffusion constant corresponding to a guest trajectory $\mathbf{r}(t)$ of N (large) MD steps with time step Δt,

$$D_{MD} = \langle \mathbf{r}^2(N\Delta t)\rangle/6N\Delta t \tag{24}$$

with D_{TST}. We used a fourth-order predictor−corrector algorithm due to Gear,[60] with a step size of $\Delta t = 0.5$ fs. Only a single guest was present in the system at any time; its velocity was originally chosen from a Gaussian distribution with the appropriate width ($\langle v^2\rangle = 3kT/m$). The speed was rescaled infrequently (either every $\Delta N = 400$ or 4000 time steps; results were found to be independent of this choice) to ensure the proper average kinetic temperature. Statistics were combined for 1000 He trajectories followed for $N = 200\,000$ steps each (with the results checked for consistency against a couple of longer, 1 ns, runs) in order to calculate the value of D_{TST} shown in Table 2. The agreement between MD and TST diffusivities is extremely good, leading one to suspect that the assumptions that underly TST are valid in this system. For example, the normalized velocity autocorrelation function for a guest is shown in Figure 5. The decay time of $\tau_{corr} \approx 2$ ps is much less than the TST cage residency time (Table 2), so an equilibrium concentration of diffusant will not be depleted from the cages by too-rapid diffusion. (Since the reaction is not energy-activated, the magnitude of E^*/k_BT is not relevant in this regard.) One should also check that the cage residency time in the dynamical simulation, τ_{rxn}, is consistent with τ_{TST}; the simulation yields $\tau_{rxn} = 26 \pm 5$ ps. While the ability of TST to predict the correct mean value is quite good, there is an extremely broad distribution (standard deviation roughly equal to the mean) of cage residency times in the simulation.

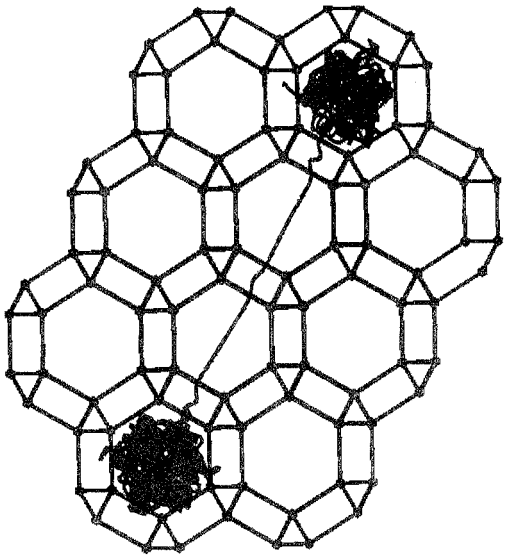

Figure 6. Trajectory corresponding to 50 ps of He motion at 300 K depicting the rare case of two sequential, correlated forward hops.

The requirement that $\tau_{corr} \ll \tau_{rxn}$ has a relevant role in the calculation of dynamical corrections to TST; the elegant techniques that have been developed to evaluate κ numerically[23,26,29] rely on this inequality holding true. Indeed, this is the case that is extremely common in situations of surface diffusion, where particles typically vibrate many times within a well before they escape. But Voter et al. have discovered[61] that if the application involves diffusion in an isotropic medium, this is not a requirement. That is, though $k(t)$ may be poorly defined for times greater than τ_{rxn}, the diffusion constant that one calculates from it in the long time limit will nevertheless be correct.

The MD simulation allows one to assess the contribution of dynamical corrections to TST to the mobility of He at room temperature. For example, one 1 ns trajectory was examined in detail. The distribution of cage residency times was, as mentioned above, quite broad. Of 36 intercage hops during that time, only one could be classified as a recrossing and that had the character of an extremely rapid reflection from a position very slightly beyond the TS surface back into the original cage, the whole process taking less than 0.02 ps. So, at least for the rigid lattice, reactive recrossings of the TS seem to be negligible for this model, and it is not necessary to find corrections via a reactive-flux calculation. More relevant to the magnitude of the diffusion constant is the existence of correlated hops between cages. Three of the 36 cage residencies were of similar duration, roughly 0.5 ps, and involved direct transits from one cage across a neighboring cage and into a second neighbor. A 50 ps fragment of the trajectory containing two such correlated hops in a row is shown in Figure 6.

The quantitative treatment of such correlated jumps, along with TS recrossings, is accounted for in the Voter−Doll formalism. One evaluates the multistate dynamical correction factor, f_d, between any two sites i and j, so that one has the correct rate, $k_{i\to j}$ for jumps between those sites:

$$k_{i\to j} = f_d(i\to j)k_{i\to} \tag{25}$$

where $k_{i\to}$ is the rate we have referred to previously as k, the rate of jumping from an initial cage to any other. If δ_{ij} is the distance between cages i and j and δ the elementary hop distance between nearest neighboring cages, eq 25 implies this correction to the TST diffusion constant:[41]

$$D = D_{\mathrm{TST}} \sum_j f_{\mathrm{d}}(i \rightarrow j) \left(\frac{\delta_{ij}}{\delta}\right)^2 \tag{26}$$

As has been observed by previous authors, distant hops are weighted by the square of the hopping distance, so one must be particularly careful not to underestimate the importance of such events.

As an alternative to the Voter−Doll formalism, one might consider this line of reasoning for our system: For a correlated random walk of N elementary steps of size δ, the mean squared displacement will be, in the limit of large N

$$\langle \mathbf{r}^2(N) \rangle = N\delta^2 (1 + 2 \sum_{k=1}^{\infty} \langle \cos \theta_{n,n+k} \rangle) \tag{27}$$

Above, $\theta_{n,n+k}$ denotes the angle between the direction of the nth jump and the $(n + k)$th. Karger and Ruthven[62] argue that $\langle \cos \theta_{n,n+k} \rangle = \langle \cos \theta \rangle^k$ where θ is the angle between successive jumps, and thus eq 27 simplifies to

$$\langle \mathbf{r}^2(N) \rangle = N\delta^2 \left(1 + \frac{2\langle \cos \theta \rangle}{1 - \langle \cos \theta \rangle}\right) \tag{28}$$

Thus, multistate dynamical corrections to TST will imply that

$$D = D_{\mathrm{TST}} \frac{1 + \langle \cos \theta \rangle}{1 - \langle \cos \theta \rangle} \tag{29}$$

The approaches of both eqs 26 and 29 require dynamical simulations in order to evaluate correction factors to D_{TST}. Of course, the former is necessary when τ_{rxn} is too long for direct MD simulation, but we can adopt the latter approach for He at 300 K, finding that $\langle \cos \theta \rangle = 0.05$. Equation 29 would then predict that dynamical effects increase the room-temperature diffusivity very slightly: $D = (1.1)D_{\mathrm{TST}}$. The fact that the correction raises the diffusivity implies that correlated forward jumps, as opposed to nonreactive reacrossings, dominate its value. Of course, one expects this value to change with temperature; as in the surface simulation of ref 53, where the average length of the "flights" which made up the trajectory grew with energy.

Unfortunately, taking D_{TST} from Table 2, one finds that this correction, though small, is in the wrong direction—D_{MD} is already slightly less than the statistically-calculated quantity, D_{TST}. A closer examination of the MD simulation reveals some discrepancies with canonical statistics. Figure 7 compares the distribution of He atoms in the doorway with the canonical distribution: $P(r) \propto r e^{(-U(r)/k_{\mathrm{B}}T)}$. (For the small region of the doorway accessible to the guest, the potential depends to a good approximation only on the radial distance, r, from the SP.) Clearly, the coordinates of the diffusant are not canonically distributed at the TS. Rather, during the brief time of its "ballistic" passage through the TS surface, He is more likely to pass near the center, and less likely to explore the sides of the doorway, than thermal equilibrium would predict. So $Q^{\ddagger}/Q_{\mathrm{A}}$ of eq 1 (alternatively, the ratio of partition functions in eq 21) will not necessarily reflect the occupancy statistics of the TS during the MD simulation. Moreover, the mean speed normal to the reaction coordinate in the TS, $\langle |v^*| \rangle_{\mathrm{MD}} = 5.0$ Å/ps, is not consistent with thermal equilibrium: $\langle |v^*| \rangle = 6.3$ Å/ps at 300 K. Interestingly, if one were to use the observed speed from MD in eq 21 (and also, though it is barely significant, apply the multistate dynamical correction factor discussed above) one would predict $D = 0.38$ Å^2/ps in complete agreement with the MD result for He at 300 K.

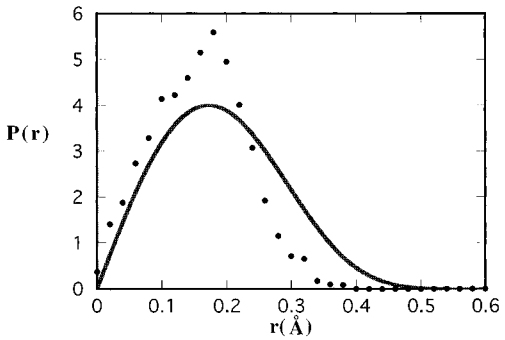

Figure 7. Probability of observing He at a distance r from the SP at 300 K. Solid line: Boltzmann probability. Circles: MD simulation, average over 100 ps trajectories of 100 atoms. Atoms are considered within the TS if they lie within a small disk of width 0.2 Å around the TS.

This issue is part of a larger problem with our attempt to produce a Maxwellian velocity distribution using microcanonical MD (with occasional velocity rescaling) in a system with so few degrees of freedom. For example, though the rms speed of He at an arbitrary location in the zeolite was correct, $\sqrt{\langle v^2 \rangle} = 7.9$ Å/ps, the mean speed was too high by about 10%; correspondingly, the distribution of velocities differed from a Gaussian. Similar issues arose in previous studies[14,63] for very low guest concentrations and rigid lattices, and they were resolved when each guest interacted with moving lattice atoms and/or other guests. A simulation with mobile lattice atoms would not only be expected to better thermalize a guest, but one expects that it would produce different results on the dynamical corrections and perhaps must importantly, via the relaxation of the lattice to a new equilibrium configuration around the guest, TST results. These effects of a moving vs rigid lattice have been observed in several previous studies.[14,40,42,63] Rather than revisit them here, we will instead take up the topic of quantum effects for He in the rigid lattice.

6. Quantum Rate of Diffusion

The phenomenon of tunneling is very much a part of our understanding of the diffusion of light impurities though solids. For example, Gillan[65] was able to explain an experimentally-observed break in the slope of the Arrhenius plot of the diffusivity of H in Nb as the onset of tunneling of H atoms between interstitial sites. Hydrogen in metals is a well-studied system about which much is understood.[66] In contrast, quantum mechanical effects in the diffusion of light guests in zeolites have been the subject of few studies. Cohen de Lara et al., in work on molecular hydrogen in zeolites, were able to show[67] that the apparent disagreement between calculated activation energies of H_2 and HD in zeolite A could be explained by making the first quantum correction to the classical Arrhenius law, the so-called Wigner−Kirkwood correction to the classical free energy.[46,68] This tunneling correction is familiar in reaction rate theory, where it is often used as a simple multiplicative correction factor to the classical rate, k_{cl}, for a barrier with imaginary frequency ν^*:

$$k = k_{\mathrm{cl}} \left(1 + \frac{1}{24}\left(\frac{h\nu^*}{k_{\mathrm{B}}T}\right)^2\right) \tag{30}$$

For He in sodalite, a classical analysis has already shown that entropy, not energy, limits transport above a certain temperature. So it is not clear whether tunneling will provide the main correction to the classical rate, except at the very lowest temperatures. Instead, one might expect that "diffraction" of

the particle through the small aperture at the TS, which might also be considered as primarily a "zero-point energy" effect, would compete with tunneling. To assess the importance of using a quantum rate theory, consider the effective diameter of this aperture. At 50 K, a plot of the Boltzmann probability density at the TS yields a diameter of roughly $^1/_2$ Å. This is also the approximate deBroglie wavelength of a He atom at 50 K. So certainly at temperatures on the order of 50 K, a quantum treatment of transport is essential. Alternatively, one might consider the zero-point energy in the TS and in the wells. For the deepest well, M2, a normal-mode analysis yields harmonic oscillation frequencies of $\nu_1 = \nu_2 = 1.5 \times 10^{12}$ s^{-1} (for oscillation parallel to plane of the O 4-ring, and therefore along the reaction coordinate) and $\nu_3 = 2.6 \times 10^{12}$ s^{-1} (perpendicular to the ring). In the TS, the frequencies of oscillation perpendicular to the reaction coordinate are $\nu^*_1 = \nu^*_2 = 7.0 \times 10^{12}$ s^{-1} and the imaginary barrier frequency is $\nu^*_3 = 1.9 \times 10^{12}$ s^{-1}. Thus, the zero-point energy for He in M2 is about 150 K, as opposed to about 300 K in the TS. While this sort of analysis overestimates the enhancement of the barrier, 150 K, due to zero-point effects (the particle is never truly localized in the plane of the TS) it indicates that such corrections may not be negligible at temperatures of order 150 K and below. As for the first-order tunneling correction, eq 30 predicts that it raises k by about 2% at 150 K and by about 14% at 50 K.

Rather than pursuing corrections to classical TST, we will calculate a reaction rate using a fully quantum TST, PI-QTST, as described in section 3. We have used standard path integral MC (PIMC)[69,70] to simulate He for temperatures between 300 and 50 K. The details of our calculation are as follows: For our temperature range and thanks to its substantial mass, the simplest implementation of PIMC,[71] a conventional Metropolis MC[72] random walk with importance sampling, was used and converged well for P in the range 20−50 (hence avoiding the large-P problem of overly stiff chains). Each MC step consisted, in the usual way, of a trial move of each individual bead with a random step uniformly chosen within a sphere of radius d, followed by acceptance of the move with probability $\max(1,e^{(E-E')/k_BT})$. E and E' were the energies (of a classical polymer chain with spring constant $Pm/\beta^2\hbar^2$) before and after the trial move, respectively. In practice, d was adjusted according to the run temperature to keep the acceptance fraction in the range of 35−70%. Values of d around 0.1 Å were typical.

To achieve the goal of calculating the ratio of partition functions in eq 15, the chain must explore the entire accessible cage volume. To this end, two standard procedures were implemented: (i) Because moves of individual beads may not be optimal for covering a large region of configuration space,[73] every few MC passes through the entire chain we performed a centroid-only move. All beads were retained in their positions relative to the centroid, which was moved a trial distance of d_c, and the move was accepted or rejected in the usual way. Values of d_c around 0.3 Å were typical. Such centroid-only moves can be considered as a rudimentary type of "staging",[70] the only type that was necessary for our application. (ii) The free energy barrier at the TS becomes progressively higher as T is lowered, making visits to the TS too infrequent for the Metropolis importance sampling algorithm to be efficient. So, centroid umbrella sampling[72,74] was used. The particle was confined to a set of nested sampling bins. Separate walks were run in each bin, with the centroid experiencing a "hard-wall" repulsion at the bin boundaries. For example, let nested volumes be as shown in Figure 8. Volume I consists of the entire cage/unit cell. Volumes II, III, ... are cylinders with their cylindrical axes centered on the TS, of sufficient diameter, 1 Å in our case, for the centroid to remain confined within them at the simulated temperature. The ratio of, for example, the partition function, $Q_{c,III}$, for a centroid-constrained polymer in III, to that of a (centroid-constrained or unconstrained; it makes little practical difference if I is the entire cage) polymer in I, $Q_{c,I}$, is

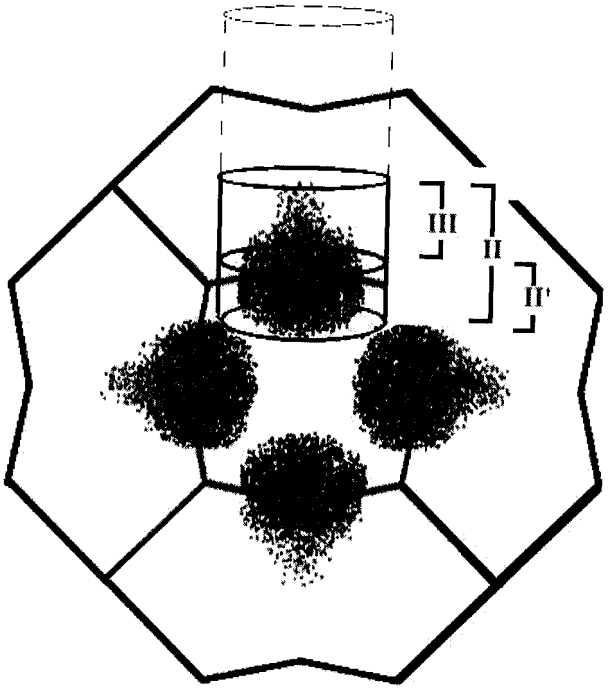

Figure 8. Dots showing the location of the centroid at each step of PIMC simulation of He at 300 K. There are $N_{II,III}$ dots within the nested volumes II, III. II and II′ are alternative sampling bins within the umbrella bin II. Whole cylinder, solid + dashed, is alternative umbrella bin.

$$\frac{Q_{c,III}}{Q_{c,I}} = \frac{Q_{c,III}}{Q_{c,II}} \frac{Q_{c,II}}{Q_{c,I}} \tag{31}$$

So if a simulation is run in I with N_I total MC steps, N_{II} of them in which the centroid falls in II, and a second simulation is run with the centroid constrained to lie entirely in II, with N_{II} total MC steps, N_{III} with the centroid falling in III, then

$$\frac{Q_{c,III}}{Q_I} \approx \frac{N_{III}}{N_{II}}\Big|_{II} \frac{N_{II}}{N_I}\Big|_{I} \tag{32}$$

where $|_V$ indicates the constraint of the centroid to bin V during the simulation. In practice, only two (as in the example above) nested umbrella bins were enough to calculate the ratio of partition functions in eq 15 to good precision.[75] N_{II} consisted of a cylinder of height 0.883 Å (1/10 of the cage diameter).

The ratio in eq 15 was evaluated numerically, in the spirit of eq 23. Thus, the smallest bin, III in the example above, can be partitioned into sampling bins indexed by their heights h, and given N_h hits in bin h, we set

$$k_{QTST} = \frac{1}{2}\langle|v^*|\rangle \lim_{h\to 0} \frac{1}{h} \frac{N_h}{N_{II}}\Big|_{II} \frac{N_{II}}{N_I}\Big|_{I} \tag{33}$$

Figure 9 shows the convergence, with h, of N_h/h. Shown are data from two independent runs (multiple runs allowed us to establish error bars), each consisting of 1.8×10^6 MC steps for a polymer with $P = 45$ beads at 50 K. Two practical notes: (i) MC statistics in the smaller sampling bins were improved if we adopted sampling regions which extended on both sides of

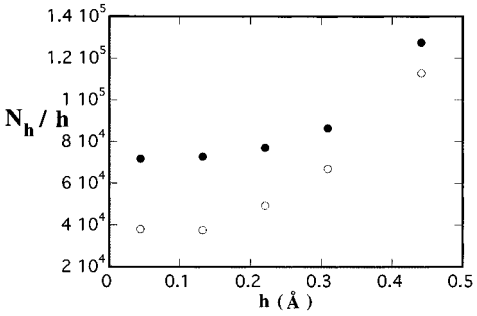

Figure 9. Number of hits in sampling bin of height h per unit height, within umbrella bin II. Two independent PIMC runs (open and filled circles) have $P = 45$ at 50 K. Data are extrapolated to $h = 0$, via a simple quadratic fit, for use in eq 33.

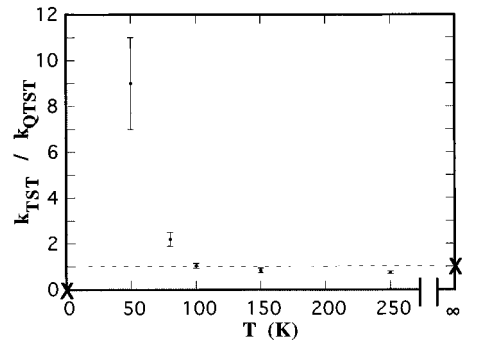

Figure 10. Ratio of the classical to quantum TST rate constants (diffusion rates) for He. Crosses at $T = 0$ and ∞ are the expected limits in the case of pure tunneling and purely classical transport, respectively.

TABLE 3: Quantum and Classical TST Rate Constants for Hopping of He in Silica Sodalite

temp (K)	k_{QTST} (ps^{-1})	k_{TST} (ps^{-1})
50	$(4.0 \pm 8) \times 10^{-5}$	3.7×10^{-4}
80	0.0011 ± 3	0.0023
100	0.0044 ± 6	0.0045
150	0.015 ± 2	0.012
250	0.043 ± 6	0.034

the TS, as by the dashed contour shown in Figure 8; (ii) adjacent bins, rather than nested bins, could also have been used for overlap regions during umbrella sampling. Adjacent bins with some region of overlap are the typical choice if the function to be sampled has only one independent variable. Such bins were used as a check on our data. That is, $N_{II'}$, the number of hits in bin II′ of Figure 8, was used in place of N_{II} in eq 33, and results were checked for consistency. But while the simple geometry of our system makes both choices reasonable for pairs of bins beyond numbers I and II, nested bins produce a more straightforward algorithm in complicated 3D, and higher dimensional, systems for which one must subdivide the reaction volume into voxels.

Classical and quantum TST hopping (diffusion) rates are given in Table 3 for several temperatures in the range 50−250 K. The ratio of these rates shows an interesting trend (Figure 10). As the temperature drops below about 100 K, the classical rate begins to rapidly exceed the quantum rate; the ratio is 9 ± 2 at 50 K. Clearly, zero-point/diffraction effects dominate at these temperatures, pulling the mobility of the guest below the classical value. Of course, this effect cannot persist indefinitely. Several aspects of the model (e.g., the suitability of a LJ form for interactions between host and guest atoms) break down and render the calculation unrealistic at very low temperatures; nevertheless, one can at least observe that the data should exhibit a turnover at very low temperatures, so that $k_{TST}/k_{QTST} \rightarrow 0$ as $T \rightarrow 0$. Temperatures above 100 K also represent a domain in which tunneling is evident, though given the height of the barrier (250 K) it is understandable that the effect is not large ($k_{TST}/k_{QTST} \approx 0.75$ at $T = 250$ K). The agreement between k_{TST} and k_{QTST} around 100 K is coincidental—a result of competition between tunneling and zero-point effects in the latter case.

One might compare the role of zero-point effects in our simulation with some found in recent surface-diffusion calculations. For example, Calhoun and Doren[76] studied CO on a Ni surface via PI-QTST, finding that zero-point effects *lowered* the effective barrier to diffusion. This was due to the details of the potential energy surface along the direction normal to the reaction coordinate; its curvature was lower at the TS than in the well. In several recent calculations of the diffusion constant for H on metal (Ni and Cu) surfaces,[77,78] one sees that quantum diffusivities exceed classical ones. An interesting exception arises in a study of H and D on Pd by Doll et al.[79] In this PI-QTST study with a nonrigid lattice, though quantum corrections to classical diffusivity are not very important for surface diffusion, they are significant for diffusion between the surface and a subsurface layer. Further, for hops between a surface state and a subsurface one, quantum rates are lower than classical ones. The authors trace this effect to the free energy for quantal degrees of freedom orthogonal to the reaction coordinate being greater at the TS than in the reactant state, just as occurs in our sodalite system. This effect is so important that, for one type of surface/subsurface pair of states, Doll et al. calculate an experimentally-observed inverse isotope effect—the diffusivity of D exceeds that of H. This effect vanishes at the lowest temperature studied (100 K), indicating that tunneling effects are beginning to dominate.

One might try to estimate a "crossover" temperature related to any competition between tunneling and zero-point effects, by comparing the size of the first tunneling correction, eq 30 to the zero-point correction found by using the quantum, rather than classical partition function ratios, i.e.,

$$\frac{Q^{\ddagger}}{Q_A} = \frac{\prod_{i=1}^{2} \frac{1}{2\sinh\left(\frac{h\nu^*_i}{2k_BT}\right)}}{\prod_{i=1}^{2} \frac{1}{2\sinh\left(\frac{h\nu_i}{2k_BT}\right)}} \quad \text{quantum} \tag{34}$$

rather than

$$\frac{Q^{\ddagger}}{Q_A} = \frac{\prod_{i=1}^{2} \left(\frac{k_BT}{h\nu^*_i}\right)}{\prod_{i=1}^{2} \left(\frac{k_BT}{h\nu_i}\right)} \quad \text{classical} \tag{35}$$

For the purposes of estimation for our system, we take well frequencies ν_i in well M2. Of course, our model does not have a single reagent well but multiple adjacent wells connected by low-lying saddles. Correspondingly, there is poor agreement between the classical partition functions evaluated using eq 35 above and numerical integration over the potential energy surface, even at 50 K. Proceeding with the argument nevertheless, we find that there is no predicted crossover. Rather, the zero-point corrections to k_{TST}, found by subtracting eq 34 from

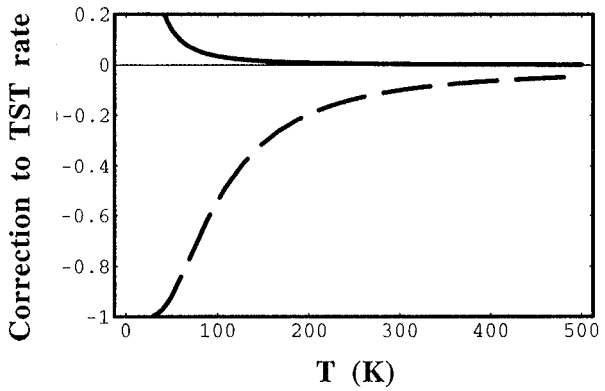

Figure 11. Fractional correction to k_{TST} arising from (solid line) tunneling correction in eq 30 and (dashed line) correction for discreteness of energy levels (so-called "zero-point energy" correction).

35, *always* dominate the tunneling corrections (see Figure 11). This result is, of course, at odds with the numerical data, pointing out the weakness of a single-well/barrier model. Perhaps it also shows the weakness of the argument that the effects of tunneling and of the discrete energy spectrum can be decoupled in a naive way, as above. Rather, a fully quantum description like PI-QTST is required to adequately characterize activated transport in a system where barriers have both an energetic and an entropic character.

7. A Centroid Pseudopotential for QTST

When one performs MC or MD sampling of partition functions, or a dynamical simulation of time correlation functions, a direct path integral calculation can be time consuming. By "direct", we mean that all beads of a quantum path interact with all surrounding particles. (If a "host" medium must be treated with path integrals as well, the problem is intensified.) A direct dynamical method of this type is the centroid molecular dynamics (CMD) approach of Cao and Voth.[80] One alternative is to develop a pairwise pseudopotential for the interaction of a quantum particle with a host. Voth and co-workers[81,82] have explored a pseudopotential CMD as an alternative to direct CMD and found it to be successful in calculating the dynamical properties of liquid parahydrogen at low temperatures.[82] This issue is particularly relevant to the activated diffusion of quantum guests in solids. For example, while a theory of dynamical corrections to TST allows us to simulate dynamics on a much shorter time scale than τ_{rxn}, suppose that τ_{corr} is itself too long for direct simulation. A classical MD simulation based on a pseudopotential may be a viable alternative when a direct MD simulation for times up to τ_{corr} is not. Similarly, a pairwise pseudopotential may allow us to simulate larger regions of a host crystal, incorporate zero-point motions of the host, or simulate a higher density of guest molecules than would be possible with direct simulation.

To adopt the approach of Voth et al.,[81,82] one begins with the definition of an effective quantum potential, or a potential of mean force on the centroid (CPMF):

$$V_c(\mathbf{x}_c) = -k_B T \ln[Z_c(\mathbf{x}_c)/Z_c^0] \tag{36}$$

The quantity $Z_c(\mathbf{x}_c)$ is the density defined in eq 14. It is a centroid-constrained partition function, with the multidimensional centroid of the path fixed at $\mathbf{x}_c$. Z_c^0 is the centroid-constrained partition function for a free particle. It has been shown[80] that the CPMF defined in this way is an effective potential for centroids, and the statistics of a classical particle in this potential field reproduce the correct centroid statistics

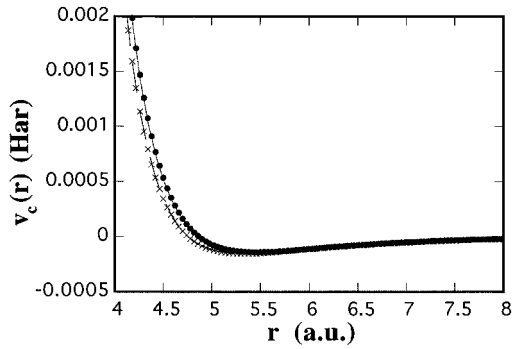

Figure 12. Effective potential energy, $v_c(r)$ from eq 38, (filled circles) for a He and O pair at separation r at 50 K; and the bare classical potential energy (crosses), both in hartrees. Lines connecting the points are fits to LJ form.

to first order in perturbation theory. Similarly, the motion of a classical particle in the force field $F_c(\mathbf{x}_c) = -dV_c(\mathbf{x}_c)/d\mathbf{x}_c$ is an approximation to the correct centroid trajectory.

A pseudopotential between the guest and host atom is constructed by letting $S = S^{rel}$ in eq 14, where

$$S^{rel}[\mathbf{x}(\tau)] = \int_0^{\hbar\beta} \left[\frac{m}{2}\dot{\mathbf{x}}^2 + u(x)\right] d\tau \tag{37}$$

$u(x)$ is the Lennard-Jones energy, eq 16, of a single guest−host pair separated by a distance x. In this case, we note the partition function as $Z_c(\mathbf{x}) = Z_c^{rel}(x)$ and define the CPMF between a guest−host centroid pair as

$$v_c(x_c) = -k_B T \ln[Z_c^{rel}(x_c)/Z_c^0] \tag{38}$$

If one assumes that the centroid pseudopotential is a superposition of such pairwise terms, we arrive at what can be called the pairwise CPMF (PPMF):

$$V_c^p(\mathbf{x}_c) \equiv \sum_i v_c(x_c^i) \tag{39}$$

where the separation between the centroid at $\mathbf{x}_c$ and the ith host atom is x_c^i. Deviations between the exact (CPMF) and pairwise (PPMF) centroid potential of mean force are due to three- and higher-body correlations of the imaginary time Feynman paths in condensed systems.

In order to construct the PPMF for He, MC sampling was performed. The range of guest−host separations $x_c = 4-12$ au was subdivided into 400 intervals and for each the centroid was constrained at the center of the interval while the potential energy $u(x)$ was sampled at all beads along the cyclic polymer. Polymer configurations were generated using importance sampling according to the action S^{rel} of eq 37. Results were generated at 50 K and, as in section 6, a moderate number of beads (around $P = 75$) was sufficient. Though it was not absolutely required, for the data presented in this section we did utilize a "threading" (sometimes referred to as a staging) algorithm.[83,84] Thus, rather than moving beads independently, sections of the chain were chosen at random and beads moved collectively according to a standard, "drifting random walk" algorithm.[84] The number of beads moved in each such threading pass was varied in order to keep the acceptance fraction at roughly 50%. 300 and 3000 passes did not yield significantly different curves $v_c(x_c)$; see Figure 12. In this figure one finds the expected zero-point energy effect in that the bare classical potential has a slightly deeper well and a minimum slightly closer to the origin than does the quantum CPMF. Were we to extend the range of the calculation toward $x_c = 0$, the shape of

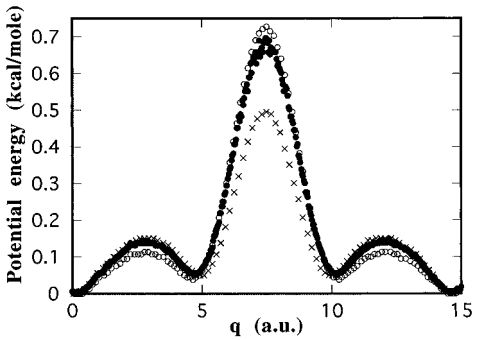

Figure 13. Potential energy as a function of distance, q, along the reaction coordinate for He in silica sodalite at 50 K. Filled circles are the CPMF, V_c, from a direct path integral simulation; open circles are the PPMF, V_c^p, of an effective classical particle, with parameters A_{eff} and B_{eff} as given in the text; and crosses are the bare classical potential energy, all in kcal/mol.

the CPMF would change significantly, reflecting the ability of the He to tunnel. But pairwise distances closer than 4 au are not relevant to thermal averages at this temperature (since 0.001 hartree $\approx$ 300 K).

The pair potential v_c was fit to a LJ form, which resulted in effective LJ parameters $A_{eff} = 6.8$ hartrees au^6 (=94 kcal/mol Å^6) and $B_{eff} = 92\,000$ hartrees au^{12} (=28 000 kcal/mol Å^{12}), which may be compared with He values in Table 1. Given the success of classical TST for classical He in silica sodalite, it is natural to forgo dynamics and simply use these parameters in eq 39 to construct the PPMF, and then find k_{TST} via quadrature as in section 5. Thus, referring back to the Eyring notation of eq 1, we propose the following approximation to the quantum TST rate constant:

$$k_{PQTST} = \frac{k_B T}{h} \frac{Q^{\ddagger}_{eff}}{Q_{A\,eff}} e^{-E^*_{eff}/k_B T} \qquad (40)$$

where the subscript "eff" indicates that it is not the bare classical potential, but the PPMF surface, V_c^p, that is being used. This yields an approximation to the rate of $k_{PQTST} = 1.9 \times 10^{-5}$ ps^{-1}. This value, being much less than k_{TST}, has the right qualitative behavior. In fact, it underestimates the direct PI-QTST rate (Table 3) by a factor of about 2.

Were we to not make the pairwise approximation but calculate the relevant partition functions "on the fly" for the polymer within the zeolite, we would be using direct PI-QTST, as prescribed in eq 15 and would obtain k_{QTST} as in section 3. In other words, the disagreement between this rate and k_{PQTST} is due to the pairwise approximation. A reaction rate can be extremely sensitive to interaction energies (here a 5−10% difference in A,B yields a factor of 20 difference in the rate). To further explore the relevance of the pairwise approximation to QTST, we can compare the direct CPMF, $V_c(\mathbf{x}_c)$, and the PPMF, $V_c^p(\mathbf{x}_c)$ along the reaction coordinate, $\mathbf{x}_c = \mathbf{q}$.

These data are shown in Figure 13. For comparison, the zeros of the data have been adjusted so that all curves agree at the global minima, M2, of potential energy. The main quantitative difference between the CPMF and classical energy occurs at the barrier; the O 6-ring presents a quantum barrier which is higher by approximately 100 K. This compares favorably with the zero-point energy difference of roughly 150 K calculated in section 6. The PPMF differs from the CPMF both in the region of the barrier and in the region between the minima M1,M2. Interestingly, the PPMF slightly overestimates the height of the barrier, while smoothing out the region (i.e., lowering the low-lying saddle energy) between these minima. These contributions would combine to lower the

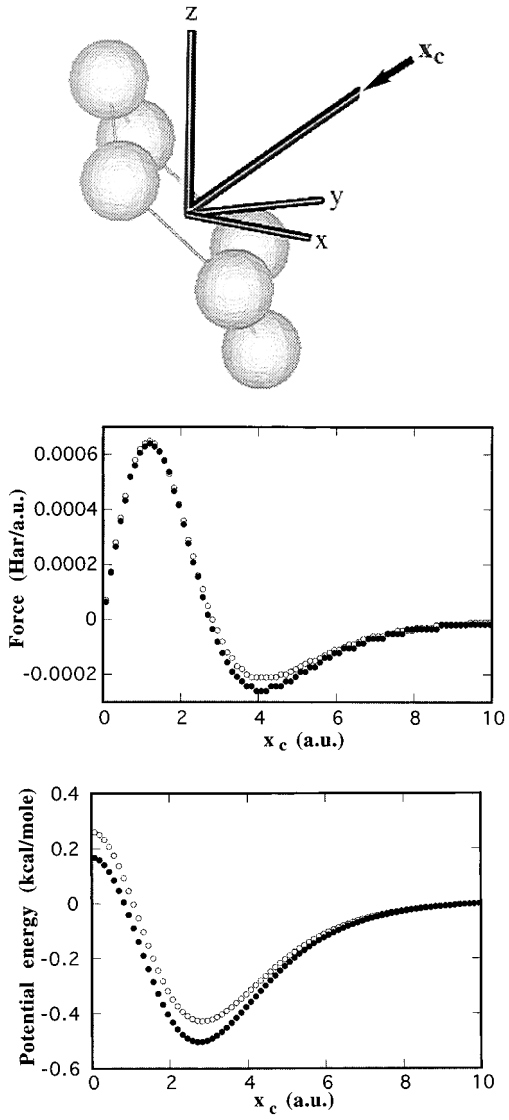

Figure 14. (a, top) Approach of centroid along the (reaction coordinate) normal to the O 6 ring. (b, middle) The mean force along the normal at distance x_c from the ring center in hartrees. Filled circles: $-\nabla V_c(x_c)$; open circles: $-\nabla V_c^p(x_c)$. (c, bottom) Potential of mean force; symbols as in Figure 13.

rate in the pair approximation. In fact, if one does the naive thing and considers the sum of these two contributions, 0.07 kcal/mol, to behave like a difference in the activation energy, E^*, then at 50 K one would predict that k_{QTST} is greater than k_{PQTST} by a factor of 2, just as one finds by direct calculation.

As an alternative to a PPMF approximations which defines an effective interaction between pairs of atoms, it may be as computationally effective and yield more accurate results to define effective interactions between the quantum particle and extended structures in the host. In a molecular liquid for example, one might calculate the effective interaction between a quantum particle and an entire liquid molecule. In our model of silica sodalite, a natural structure of interest is the O 6-ring which delineates the TS. In fact, the sodalite cage potential can be completely constructed from the 24 O atoms of four such rings. One would then define a PPMF between the guest and the host ring as in eq 38, $v_c^{ring}(\mathbf{x}_c,\theta)$, where $\mathbf{x}_c$ is the vector from the center of an oriented ring to the centroid, which makes an angle θ with the ring plane.[85] Figure 14a shows this ring with the guest approaching normally ($\theta = 90°$). Figure 14b shows the effective force $-\nabla V_c^p$ in the pairwise approximation for this approach, as well as the directly calculated centroid

force, $-\nabla V_c \equiv -\nabla v_c^{ring}$. These data indicate that the pair approximation errs mainly by underestimating the magnitude of the net attractive force at centroid locations near (about 4 au from) the ring. The pair approximation does a very good job of predicting (only slightly overestimating) the repulsive peak closer to the ring, as well as its decay toward zero at the ring center. One presumes that overestimate leads to the overestimate of the barrier height by the PPMF in Figure 13. (See Figure 14c, which shows the CPMF and PPMF corresponding to the forces in Figure 14b). It remains to be seen whether a representation of the zeolite as a collection of 6-rings, and use of the corresponding PPMF, v_c^{ring}, would reproduce the reduction of the low-lying barriers as well, leading to a more accurate prediction of the reaction rate, k_{QTST}. This question is left open for future study.

8. Conclusions

The diffusive transport of noble gases through the siliceous form of sodalite was modeled using semiempirical potentials and classical and quantum TST. For a range of temperatures around room temperature, classical TST predicts energy-activated, hopping transport of Ne and Ar. When classical TST is applied to He, transport is found to be limited by the entropy difference between the caged state and the transition state for temperatures above roughly 50 K. Microcanonical MD simulations indicate that He is trapped in sodalite cages for a time on the order of 20 ps at room temperature, in excellent agreement with the TST prediction. A quantum-mechanical treatment of He is necessary below room temperature, and tunneling and zero-point effects compete to modify the diffusion constant. Below about 100 K, zero-point effects begin to dominate, and at 50 K the diffusion constant from path integral quantum TST is roughly a factor of 9 lower than classical TST would predict. Finally, a centroid pseudopotential was developed in order to speed quantum TST or dynamical calculations. It does a very good job of reproducing the centroid potential of mean force at 50 K, and hence a good job, as compared with a full path integral QTST calculation, of predicting the rate of He transport.

Acknowledgment. We thank E. Cohen de Lara, R. Hernandez, J. E. Straub, and A. F. Voter for very helpful conversations and J. Boccio, A. Calhoun, J. Cao, E. Engstrom, M. Pavese, and B. Yanoff for technical contributions. A. B. is grateful to B. J. Berne for guidance and support during her introduction to this field of research. We gratefully acknowledge financial support from the Research Corporation Award C-3617, Howard Hughes Medical Institute Fund, Faculty Research Fund and Lang Fund of Swarthmore College, and C90 computing time from the Pittsburgh Supercomputing Center.

References and Notes

(1) *Zeolites: Science and Technology*; Ribeiro Ramoa, F., Rodrigues, A. E., Rollmann, L. D., Naccache, C., Eds.; Nijhoff: Boston, 1984. Bhatia, S. *Zeolites Catalysis: Principles and Applications*; CRC Press: Boca Raton, FL 1990. Suib, S. L. *Chem. Rev.* **1993**, *93*, 803.

(2) For example: Karger, J.; Ruthven, D. M. *Diffusion in Zeolites and other Microporous Solids*; John Wiley and Sons: New York, 1992. Xiao, J.; Wei, J. *Chem. Eng. Sci.* **1992**, *47*, 1123, 1143. Chen, N. Y.; Degnan Jr., T. F.; Smith, C. M. *Molecular Transport and Reaction in Zeolites*; VCH Publishers: New York, 1994.

(3) Ozin, G. A.; Kuperman, A.; Stein, A. *Angew. Chem., Int. Ed. Engl.* **1989**, *28*, 359. Stucky, G. D.; Srdanov, V. I.; Harrison, W. T. A.; Gier, T. E.; Keder, N. L.; Moran, K. L.; Haug, K.; Metiu, H. I. In *Supramolecule Architecture: Synthetic Control in Thin Films and Solids*; Bein, T., Ed.; American Chemical Society: Washington, DC, 1992.

(4) Weitkamp, J.; Fritz, M.; Ernst, S. In *Proceedings from the Ninth International Zeolite Conference: II*; von Ballmoos, R., Higgins, J. B., Treacy, M. M. J., Eds.; Butterworth Heinemann: Boston, 1992.

(5) Monson, P. R. *Energy Res. Abstr.* **1982**, *7*, No. 42509.

(6) Fraissard, J.; Ito, T. *Zeolites* **1988**, *8*, 350. Tsiao, C.; Kauffman, J. S.; Corbin, D. R.; Abrams, L.; Carroll Jr., E. E.; Dybowski, C. *J. Phys. Chem.* **1991**, *95*, 5586. Jameson, C. *J. Chem. Phys.* **1996**, *104*, 1709.

(7) Barrer, R. M. *Zeolites and Clay Minerals as Adsorbers and Molecular Sieves*; Academic Press: London, 1978; Chapter 11.

(8) Walker, P. L., Jr.; Austin, L. G.; Nandi, S. P. *Chem. Phys. Carbon* **1966**, *2*, 257.

(9) Rutheven, D. M. *Principles of Adsorption and Adsorption Processes*; John Wiley and Sons: New York, 1984; Chapter 5.

(10) Pollard, W. G.; Present, R. D. *Phys. Rev.* **1948**, *73*, 762.

(11) Hill, T. L. *Introduction to Statistical Thermodynamics*; Addision Wesley: Reading, MA, 1960; p 172. Ruthven, D. M.; Doetsch, I. H. *J. Chem. Soc., Faraday Trans. 1* **1976**, *72*, 1043.

(12) The physadsorption of guests at preferred sites, with the corresponding activation energies controlling diffusion, can be inferred from numerous studies. Spectroscopic studies like: Cohen De Lara, E.; Kahn, R. In *Guidelines for Mastering the Properties of Molecular Sieves*; Barthomeuf, D., et al., Eds.; Plenum Press: New York, 1990; p 169, or data on H_2 and CH_4 summarized in: Jobic, H. *Spectrochim. Acta* **1992**, *48A*, 293, and molecular dynamics studies like: Demontis, P.; Yashonath, S.; Klein, M. L. *J. Phys. Chem.* **1989**, *93*, 5016; Cohen De Lara, E.; Goulay, A. M. *J. Chem. Phys.* **1989**, *90*, 7482; or Yashonath, S.; Santikary, P. *Mol. Phys.* **1993**, *78*, 1 provide some examples.

(13) Some representative studies: Hufton, J. R. *J. Phys. Chem.* **1991**, *95*, 8836. Catlow, C. R. A.; Freeman, C. M.; Vessal, B.; Tomlinson, S. M.; Leslie, M. *J. Chem. Soc., Faraday Trans.* **1991**, *87*, 1947. Goodbody, S. J.; Watanabe, K.; MacGowan, D.; Walton, J. P. R. B.; Quirke, N. *Ibid.* **1991**, *87*, 1951. June, R. L.; Bell, A. T.; Theodorou, D. N. *J. Phys. Chem.* **1992**, *96*, 1051. Nicholas, J. B.; Trouw, F. R.; Mertz, J. E.; Iton, L. E.; Hopfinger, A. J. *J. Phys. Chem.* **1993**, *97*, 4149.

(14) June, R. L.; Bell, A. T.; Theodorou, D. N. *J. Phys. Chem.* **1991**, *95*, 8866.

(15) El Amrani, S.; Vigne-Maeder, F.; Bigot, B. *J. Phys. Chem.* **1992**, *96*, 9418.

(16) See the recent review by Hanggi, P.; Talkner, P.; Borkovec, M. *Rev. Mod. Phys.* **1990**, *62*, 251 and references therein.

(17) Laidler, K. J.; King, M. C. *J. Phys. Chem.* **1983**, *87*, 2657.

(18) Eyring, H. *J. Chem. Phys.* **1935**, *3*, 107.

(19) Evans, M. G.; Polyani, M. *Trans. Farad. Soc.* **1935**, *31*, 875. Wigner, E. *Trans. Faraday Soc.* **1938**, *34*, 29.

(20) Laidler, K. J.; Tweedale, A. *Adv. Chem. Phys.* **1971**, *21*, 113.

(21) Pollak, E.; Child, M. S.; Pechukas, P. *J. Chem. Phys.* **1980**, *72*, 1669.

(22) Keck, J. C. *Adv. Chem. Phys.* **1967**, *13*, 85. Pechukas, P. In *Dynamics of Molecular Collisions*; Miller, W. H., Ed.; Plenum: New York, 1976; Part B. Pollak, E. In *Theory of Chemical Reaction Dynamics*; Baer, M., Ed.; CRC Press: Boca Raton, FL, 1985; Vol. IV. Tucker, S. C. In *New Trends in Kramers Reaction Rate Theory*; Talkner, P., Hangii, P., Eds.; Kluwer Academic: Boston, 1995; p 5.

(23) Chandler, D. *J. Chem. Phys.* **1978**, *68*, 2959.

(24) Chandler, D.; Pratt, L. R. *J. Chem. Phys.* **1976**, *65*, 2925. Hynes, J. T. In *Theory of Chemical Reaction Dynamics*; Baer, M., Ed.; CRC Press: Boca Raton, FL, 1985; Vol. IV.

(25) Kramers, H. A. *Physica* **1940**, *4*, 284.

(26) Berne, B. J.; Borkovec, M.; Straub, J. E. *J. Phys. Chem.* **1988**, *92*, 3711.

(27) A related quantity is the "conversion coefficient" of Anderson (Anderson, J. B. *J. Chem. Phys.* **1973**, *58*, 4684), which is the ratio of successful, reactive crossings to all crossings of the *TS*.

(28) Chandler, D. *Introduction to Modern Statistical Mechanics*; Oxford University: New York, 1987; Chapter 8.

(29) Berne, B. J. In *Multiple Time Scales*; Brackbill, J. V., Cohen, B. I., Eds.; Academic Press: New York, 1985. Montegomery, J. A.; Chandler, D.; Berne, B. J. *J. Chem. Phys.* **1979**, *70*, 4056. Straub, J. E.; Hsu, D. A.; Berne, B. J. *J. Phys. Chem.* **1985**, *89*, 5188.

(30) Vinyard, G. *J. Phys. Chem. Solids* **1957**, *3*, 121. Franklin, W. M. In *Diffusion in Solids: Recent Developments*; Nowick, A. S., Burton, J. J., Eds.; Academic Press: New York, 1975; p 1. Snurr, R. Q.; Bell, A. T.; Theodorou, D. N. In *Zeolite Science 1994: Recent Progress and Discussions*; Karge, H. G., Weitkamp, J., Eds.; Elsevier Science: New York, 1995.

(31) Bennett, C. H. p 73.

(32) Wert, C.; Zener, C. *Phys. Rev.* **1949**, *76*, 1169.

(33) Wert, C. A. *Phys. Rev.* **1950**, *79*, 601.

(34) Rice, S. A. *Phys. Rev.* **1958**, *112*, 804.

(35) Ruthven, D. M.; Derrah, R. I. *Trans. Faraday Soc.* **1972**, *68*, 2332.

(36) Barrer, R. M. *Trans. Faraday Soc.* **1941**, *37*, 590. Ruthven, D. M. *Can. J. Chem.* **1974**, *52*, 3523. Theodorou, D.; Wei, J. *J. Catal.* **1983**, *83*, 205.

(37) Sargent, R. W. H.; Whitford, C. J. In *Molecular Sieve Zeolites II*; Gould, R. I., Ed.; American Chemical Society: Washington, DC, 1971; p 144. Betemps, M.; Jutard, A. *J. Phys. D: Appl. Phys.* **1980**, *13*, 423.

(38) Banavar, J. R.; Cohen, M. H.; Gomer, R. *Surf. Sci.* **1981**, *107*, 113.

(39) Barrer, R. M.; Jost, W. *Trans. Faraday Soc.* **1949**, *45*, 928.

(40) Voter, A. F.; Doll, J. D. *J. Chem. Phys.* **1984**, *80*, 5814, 5832.

(41) Voter, A. F.; Doll, J. D. *J. Chem. Phys.* **1985**, *82*, 80.

(42) Zhang, Z.; Haug, K.; Metiu, H. *J. Chem. Phys.* **1990**, *93*, 3614.
(43) Yashonath, S.; Santikary, P. *J. Phys. Chem.* **1993**, *97*, 3849.
(44) See the reviews of: Miller, W. H. *Acc. Chem. Res.* **1976**, *9*, 306. Pechukas, P. *Annu. Rev. Phys. Chem.* **1981**, *32*, 159. Truhlar, D. G.; Hase, W. L.; Hynes, J. T. *J. Phys. Chem.* **1983**, *87*, 2664.
(45) Voth, G. A.; Chandler, D.; Miller, W. H. *J. Chem. Phys.* **1989**, *91*, 7749. Voth, G. A. *J. Phys. Chem.* **1993**, *97*, 8365.
(46) Feynman, R. P.; Hibbs, A. R. *Quantum Mechanics and Path Integrals*; McGraw-Hill: New York, 1965; Chapter 10.
(47) Feynman, R. P. *Statistical Mechanics*; Benjamin/Cummings: Reading, MA, 1972; Chapter 3.
(48) Chandler, D.; Wolynes, P. G. *J. Chem. Phys.* **1981**, *74*, 4078.
(49) Gillan, M. J. *J. Phys. C* **1987**, *20*, 3621. Additionally, Valone, Voter, and Doll (ref 77) used what amounts to a variational approximation to PI-QTST; see: Voth, G. A. *J. Chem. Phys.* **1991**, *94*, 4095.
(50) Richardson Jr., J. W.; Pluth, J. J.; Smith, J. V.; Dytrych, W. J.; Bibby, D. M. *J. Phys. Chem.* **1988**, *92*, 243.
(51) Kiselev, A. V.; Lopatkin, A. A.; Shulga, A. A. *Zeolites* **1985**, *5*, 261.
(52) Wahnstrom, G.; Haug, K.; Metiu, H.; *Chem. Phys. Lett.* **1988**, *148*, 158. Haug, K.; Wahnstrom, G.; Metiu, H. *J. Chem. Phys.* **1989**, *90*, 540.
(53) Sholl, D. S.; Skodje, R. T. *Physica D* **1994**, *71*, 168.
(54) Machta, J.; Zwanzig, R. *Phys. Rev. Lett.* **1983**, *50*, 1959.
(55) Jameson, C. J.; Jameson, A. K.; Gerald, R. II; de Dios, A. C. *J. Chem. Phys.* **1992**, *96*, 1676. Auerbach, S. M.; Henson, N. J.; Cheetham, A. K.; Metiu, H. I. *J. Phys. Chem.* **1995**, *99*, 10600.
(56) Zhou, H-X.; Zwanzig, R. *J. Chem. Phys.* **1991**, *94*, 6147.
(57) Voter, A. F. *J. Chem. Phys.* **1985**, *82*, 1890.
(58) Barrer, R. M.; Vaughan, D. E. W. *J. Phys. Chem. Solids* **1971**, *32*, 731.
(59) Nicholas, J. B.; Hopfinger, A. J.; Trouw, F. R.; Iton, L. E. *J. Am. Chem. Soc.* **1991**, *113*, 4792.
(60) Evans, D. J.; Morriss, G. P. *Comput. Phys. Rep.* **1984**, *1*, 297.
(61) Voter, A. F. *Phys. Rev. Lett.* **1989**, *63*, 167. Voter, A. F.; Doll, J. D.; Cohen, J. M. *J. Chem. Phys.* **1989**, *90*, 2045.
(62) Karger, J.; Ruthven, D. M. *Diffusion in Zeolites and other Microporous Solids*; John Wiley and Sons: New York, 1992; Chapter 2.
(63) Demontis, P.; Fois, E. S.; Suffritti, G. B.; Quartieri, S. *J. Phys. Chem.* **1990**, *94*, 4329.
(64) Demontis, P.; Suffritti, G. B.; Fois, E. S.; Quartieri, S. *J. Phys. Chem.* **1992**, *96*, 1482.
(65) Gillan, M. J. *Phys. Rev. Lett.* **1987**, *58*, 563.
(66) See for example Volkl, J.; Alefeld, G. In *Diffusion in Solids: Recent Developments*; Nowick, A. S., Burton, J. J., Eds.; Academic Press: New York, 1975. *Electronic Structure and Properties of Hydrogen in Metals*; Jena, P., Satterthwaite, C. B., Eds.; Plenum: New York, 1983. *Metal-Hydrogen Systems: Fundamentals and Applications*; Marchester, F. D., Ed.; Elsevier Sequoia: Lausanne, France, 1990; Vol. I.
(67) Bouchard, J. P.; Cohen De Lara, E.; Kahn, R. *Europhys. Lett.* **1992**, *17*, 583.
(68) Landau, L.; Lifschitz, E. *Statistical Physics, Vol. 1*; Pergamon Press: New York, 1980; Chapter 33.
(69) Some reviews on path integral techniques are: Berne, B. J.; Thirumalai, D. *Annu. Rev. Phys. Chem.* **1987**, *37*, 401. Doll, J. D.; Freeman, D. L.; Beck, T. L. *Adv. Chem. Phys.* **1990**, *78*, 61. Ceperley, D. *Rev. Mod. Phys.* **1995**, *67*, 279.
(70) Sprik, M.; Klein, M.; Chandler, D. *Phys. Rev. B.* **1985**, *31*, 4234.
(71) Allen, M. P.; Tildesley, D. J. *Computer Simulation of Liquids*; Clarendon Press: Oxford, U.K., 1987; Chapter 10.
(72) Reference 71, Chapter 4. Valleau, J. P.; Whittington, S. G. In *Statistical Mechanics*; Berne, B. J., Ed.; Plenum: New York, 1977; Part A.
(73) Hall, R. W.; Berne, B. J. *J. Chem. Phys.* **1984**, *81*, 3641.
(74) Reference 28, Chapter 6.
(75) Were we working at extremely low temperatures, a large number of umbrella bins would be necessary. At some point, rather than perform numerous MC samplings in intermediate bins, it might be more efficient to implement, e.g., the MC method of ref 57 involving occasional large displacements specifically designed to take one from a well into the TS.
(76) Calhoun, A.; Doren, D. *J. Phys. Chem.* **1993**, *97*, 2251.
(77) Valone, S. M.; Voter, A. F.; Doll, J. D. *Surf. Sci.* **1985**, *155*, 687; *J. Chem. Phys.* **1986**, *85*, 7480.
(78) Lauderdale, J. G.; Truhlar, D. G. *J. Am. Chem. Soc.* **1985**, *107*, 4590; *Surf. Sci.* **1985**, *164*, 558. Haug, K.; Wahnstrom, G.; Metiu, H. *J. Chem. Phys.* **1990**, *92*, 2083. Haug, K.; Metiu, H. *J. Chem. Phys.* **1991**, *94*, 3251. Sun, Y-C.; Voth, G. A. *J. Chem. Phys.* **1993**, *98*, 7451.
(79) Rick, S. W.; Lynch, D. L.; Doll, J. D. *J. Chem. Phys.* **1993**, *99*, 8183.
(80) Cao, J.; Voth, G. A. *J. Chem. Phys.* **1994**, *100*, 5093, 5106. Cao, J.; Voth, G. A. *J. Chem. Phys.* **1994**, *101*, 6157.
(81) Cao, J.; Voth, G. A. *J. Chem. Phys.* **1994**, *101*, 6168.
(82) Pavese, M.; Voth, G. A. *Chem. Phys. Lett.* **1996**, *249*, 231.
(83) Jacucci, G.; Omerti, E. *J. Chem. Phys.* **1983**, *79*, 3051.
(84) Pollock, E. L.; Ceperley, D. M. *Phys. Rev. B* **1984**, *30*, 2555.
(85) In fact, the 6-rings are not formed of coplanar atoms in silica sodalite (though the 4-rings are). But one can define a plane from which the deviations of the O positions average to zero; this is the plane of the TS.